INFERRING RADAR SCATTERING FROM LUNAR SURFACE. A. K. Virkki[1] and S. S. Bhiravarasu[2], [1]Arecibo Observatory/University of Central Florida, HC-3 Box 53995, Arecibo, PR-00612, USA, anne@naic.edu. [2]Lunar and Planetary Institute/Universities Space Research Association, 3600 Bay Area Blvd, Houston, TX-77058, USA, sbhiravarasu@usra.edu.

Introduction: High radar reflectivity has been linked to thick water ice deposits in some Solar System objects such as the permanently shadowed polar regions (PSRs) of Mercury and Jovian satellites [1-3]. However, radar detection of water ice in the permanently shadowed regions near the poles of the Moon has been a topic of intense debate since several years [4-7]. Apart from the ground-based planetary radar systems, since 2008, two orbital miniature synthetic aperture radars on the Chandrayaan-1 and Lunar Reconnaissance Orbiter (LRO) missions (Mini-SAR and Mini-RF respectively) have imaged the lunar surface with the main purpose of detecting the distinctive radar polarimetric signature of ice deposits at the lunar poles. Both ground-based and orbital-based high resolution radar data showed that the anomalously high radar reflectivity observed from PSRs on the Moon is not unique to the poles, and also suggested a source other than accumulations of thick water ice deposits (e.g. [6-8])

The majority of existing literature for interpreting lunar radar scattering is based on empirical models [9,10,11]. These models are useful for describing the overall radar scattering of a target, but not for locations with anomalously high abundance of wavelength scale particles. Also, the role of single-scattering effects by irregular wavelength-scale particles on the observed echo is remarkably underrepresented in the existing literature. Virkki and Muinonen [12] have presented how irregular wavelength-scale particles on planetary surfaces affect the radar echo, but many questions related to the scattering processes remain to be addressed. We discuss how cm-to-dm-scale ice particles on the Lunar surface would appear in the radar images obtained by the Mini-RF radar instrument as compared to rock particles. We demonstrate the roles that the shape, the size distribution form and range, and the composition of the wavelength-scale particles (the "rubble" or "cobbles") play in the radar echoes. Scattering by the surface particles is especially relevant to the shorter (<13-cm) wavelength radar signals that penetrate only from centimeters to decimeters into the Lunar surface.

Methods: We analyze the S-band (12.6-cm wavelength) radar imaging data obtained by the Mini-RF instrument and compare the observed radar albedo data distributions to numerical simulations of radar scattering by irregular wavelength-scale particles. The Mini-RF radar receiver detects an echo scattered from the Lunar surface simultaneously in two linear orthogonal polarization states from which we can compute the echo power in two circular polarizations [13]. The opposite-circular (OC) polarization as compared to the transmitted signal is composed of both specular and diffuse scattering returns, whereas the same-circular (SC) polarization component arises only from scattering by asymmetric particles or multiple-scattering events. Diffuse scattering of radar signals may take place due to the presence of features such as rocks, small hills, valleys, and crater ejecta, or wavelength-scale particles within the probing depth of the radar. At low radar incidence angles (the angle between the incident direction and the normal to the surface at the point of intercept), the OC returns are dominated by quasi-specular scattering, and at higher incidence angles, the OC echoes are produced by scattering from radar-facing facets as well as by diffuse scattering from wavelength-scale roughness.

The radar cross section (σ) is derived by integrating the received power (P_R) with regard to the transmitted power (P_T), the wavelength (λ), the distance of the target (d_t), and the antenna gain (G_A) [14]:

$$\sigma = ((4\pi)^3 \, d_t^4 \, P_R)/(G_A^2 \, \lambda^2 \, P_T). \quad (1)$$

The radar cross section divided by the geometric cross section (projected area of the target or the observed area) at the time of the observation, gives us the radar albedo (σ^0). The radar albedo is by definition the reflectivity of the target compared to an ideally conducting metallic sphere with an equal projected area and located at an equal distance.

The circular-polarization ratio (μ_C), or the ratio of σ in the SC polarization sense to σ in the OC polarization sense has been traditionally used as a first-order measure of the wavelength-scale near-surface roughness (e.g., [14,15] The main strength of the circular-polarization ratio is that it can be obtained easily without knowledge of the contributing projected area, and nearly all the systematic errors are cancelled out in the ratio. Therefore, μ_C is one of the most commonly analyzed parameters in Lunar radar research, as it is considered to not only give implications of near-surface roughness, but also to detect and characterize potential water ice deposits in the PSRs [6,8,15]. The μ_C values have also been linked to the

boulder counts around young, fresh impact craters [16], and have been shown to decrease as a function of crater age [15].

Instead of μ_C, we study the correlation between the radar albedos in the two orthogonal circular polarizations. We selected 28 craters, and classified them into four categories: polar anomalous, polar fresh, non-polar anomalous, and non-polar fresh. We selected 4,000-10,000 sample pixels from each area of interest and plotted the OC radar albedo on the vertical axis and the SC radar albedo on the horizontal axis, as shown as an example in Fig. 1.

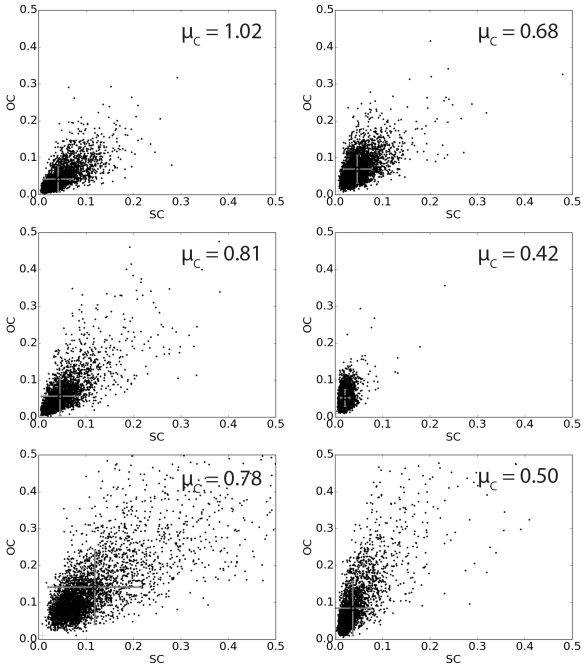

Figure 1. The opposite-circular (OC) and same-circular (SC) polarization observed by the Mini-RF instrument for three non-polar anomalous craters: Byrgius C, Cardanus E, and Gardner. On the left, we have selected data points internal to the crater rim, and on the right, external to the crater rim.

Results: We find that the average circular-polarization ratio is not uniquely indicative of the extent of the SC radar albedo distribution, which is a direct measure of the abundance of rubble in the craters. Better indicator is the standard deviation of the SC radar albedo distribution, or parameters that are better descriptive of the cone-shaped data distribution forms. We show that general radar scattering laws alone are not sufficient to model the radar albedo distribution on the crater floors and the surrounding ejecta, but an additional component is required to model the radar signature of the cm-to-dm-scale rubble so that

$$\sigma^0 = P_c\,\sigma^0_c + (1\text{-}P_c)\,\sigma^0_s \qquad (2)$$

where σ^0 is the observed total radar albedo, σ^0_c is the effective radar albedo of all the contributing particles (radius from 0.5 cm to ~ 40 cm, power-law size distribution index ~2.2–4.2) within a pixel in a Mini-RF image (~30 m x 15 m), P_c is the fraction of the radar echo that scattered from the contributing particles, and σ^0_s is the radar albedo of the bulk surface (based on a general radar scattering law such as the Bragg approximation [11]).

The results strongly suggest that ice is indistinguishable from silicate-rich material in radar images unless we can be certain that the shape of the particles follows directly from the abundance of ice in the particles. Our numerical computations show that the particle shape plays a greater role in the radar signature than the mineralogic composition, which is crucial information for understanding the cause of the anomalously high circular-polarization ratios.

References: [1] Ostro, S. J. et al. (1992) *JGR,* 97, 18227. [2] Black G. J. et al. (2001) *Icarus, 151,* 167-180, [3] Harmon, J. K. et al. (2011) *Icarus,* 211, 37-50. [4] Nozette, S. et al. (2001) *JGR,* 106, 23253-23266). [5] Campbell B. A. et al. (2006) *Nature,* 443, 835-837. [6] Spudis P. D. et al. (2013) *JGR,* 118, 2016-2029. [7] Fa W. and Cai Y. (2013) *JGR,* 118, 1-27. [8] Thomson B. J. (2012) *GRL,* 39, L14201. [9] Hagfors T. (1964) *JGR,* 69, 3779-3784. [10] Thompson T. W. et al. (2011) *JGR,* 116, E01006. [11] Ulaby F. T. et al. (1982) *Microwave Remote Sensing II*, Artech House. [12] Virkki A. K. and Muinonen K. O. (2016), *Icarus,* 269, 38-49. [13] Raney R. K. et al. (2011) *Proc. of the IEEE* 99(5). [14] Ostro, S. J. (1993) *Rev. of Mod. Phys.,* 65(4), 1235-1295. [15] Campbell B. A. et al. (2010) *Icarus,* 208, 565-573. [16] Li. Y. et al. (2017) *LPS XLVIII,* Abstract #1413.

Acknowledgements: This research was supported by NASA's Near-Earth Object Observations Program through grant no. NNX13AQ46G awarded to Universities Space Research Association for the Arecibo Planetary Radar Program and, after April 2018, through grant no. 80NSSC18K1098 awarded to the University of Central Florida (UCF). This work was also partially supported by NASA through the Solar System Exploration Research Virtual Institute under grant number NNA09DB33A. The Arecibo Observatory is a facility of the National Science Foundation operated under cooperative agreement by UCF, Yang Enterprises, Inc., and Universidad Ana G. Méndez.